1-1-2014

Edge-enriched graphene quantum dots for enhanced photo-luminescence and supercapacitance

Mahbub Hassan
University of Sydney

Enamul Haque
University of Sydney

Kakarla Raghava Reddy
University of Sydney

Andrew I. Minett
University of Sydney, aminett@uow.edu.au

Jun Chen
University of Wollongong, junc@uow.edu.au

See next page for additional authors

Edge-enriched graphene quantum dots for enhanced photo-luminescence and supercapacitance

Abstract

Graphene quantum dots (GQDs) with their edge-bound nanometer-size present distinctive properties owing to quantum confinement and edge effects. We report a facile ultrasonic approach with chemical activation using KOH to prepare activated GQDs or aGQDs enriched with both free and bound edges. Compared to GQDs, the aGQDs we synthesized had enhanced BET surface area by a factor of about six, the photoluminescence intensity by about four and half times and electro-capacitance by a factor of about two. Unlike their non-activated counterparts, the aGQDs having enhanced edge states emit enhanced intense blue luminescence and exhibit electrochemical double layer capacitance greater than that of graphene, activated or not. Apart from their use as part of electrodes in a supercapacitor, the superior luminescence of aGQDs holds potential for use in biomedical imaging and related optoelectronic applications.

Keywords

luminescence, photo, enhanced, supercapacitance, dots, edge, quantum, graphene, enriched

Disciplines

Engineering | Physical Sciences and Mathematics

Publication Details

Hassan, M., Haque, E., Reddy, K. Raghava., Minett, A. I., Chen, J. & Gomes, V. G. (2014). Edge-enriched graphene quantum dots for enhanced photo-luminescence and supercapacitance. Nanoscale, 6 (20), 11988-11994.

Authors

Mahbub Hassan, Enamul Haque, Kakarla Raghava Reddy, Andrew I. Minett, Jun Chen, and Vincent G. Gomes

Edge-enriched graphene quantum dots for enhanced photo-luminescence and supercapacitance†

Mahbub Hassan,[a] Enamul Haque,[b] Kakarla Raghava Reddy,[a] Andrew I. Minett,[b] Jun Chen[c] and Vincent G. Gomes*[a]

Graphene quantum dots (GQDs) with their edge-bound nanometer-size present distinctive properties owing to quantum confinement and edge effects. We report a facile ultrasonic approach with chemical activation using KOH to prepare activated GQDs or aGQDs enriched with both free and bound edges. Compared to GQDs, the aGQDs we synthesized had enhanced BET surface area by a factor of about six, the photoluminescence intensity by about four and half times and electro-capacitance by a factor of about two. Unlike their non-activated counterparts, the aGQDs having enhanced edge states emit enhanced intense blue luminescence and exhibit electrochemical double layer capacitance greater than that of graphene, activated or not. Apart from their use as part of electrodes in a supercapacitor, the superior luminescence of aGQDs holds potential for use in biomedical imaging and related optoelectronic applications.

Introduction

The development of new types of graphene quantum dots (GQDs), *e.g.*, with edge enrichment, opens new horizons for the design and fabrication of devices with enhanced optical and electrochemical properties.[1] Recent advances in GQD synthesis are mainly based on their surface states.[2] Yet the origin of photoluminescence (PL) in GQDs, whether stemming from emissive surface traps[3] or edge-states[4] remains unresolved. Recently, based on their comprehensive work, Lingam *et al.*[5] concluded that rather than functional groups, the random structure of their edges mainly contributes towards their PL. Due to its luminescence and band gap tuning capabilities, GQDs have been receiving substantial interest for application in biomedical imaging[6] and photovoltaics.[1] However, their potential as electrode materials in electrochemical energy storage devices is yet to receive much attention. In particular, the spherical shape and reduced size of GQDs offer greater proportion of edge sites compared to graphene and this could lead to enhanced adsorption of ionic charges[7] crucial in supercapacitance applications.

Activation of carbon nanomaterials with chemical reagents can effectively tune their intrinsic properties, including the electronic, surface and local chemical characteristics.[8] KOH is suitable for chemical activation and has been used in activated carbons to produce well-de□ned micropore distribution, and signi□cant enhancements in micropore volume and speci□c surface areas of up to 3000 $m^2\ g^{-1}$.[9] For instance, KOH activated carbon nanotubes have shown enhanced electrochemical energy storage potential for use in supercapacitors.[10] Activation of 2D graphene sheets with KOH has the potential to enable creation of activated edges at both the free ends and pores to impart exceptional properties.[11] Recent developments with graphene edge-enrichment have generated much research excitement[12] since the edge-plane atoms exhibit signi□cantly higher electron transfer rates compared to basal planes on both highly ordered pyrolytic graphite as well as multi-layered graphene.[13] As in free-end edges, the pore edges of graphene function as active ion scavenging sites to produce robust electrochemical double layer capacitance (EDLC).[14]

In view of the remarkable edge effects of 0D GQDs,[15] activated GQDs with both exposed free and bound edges offer more active sites and could dramatically alter their electronic characteristics and produce new phenomena and unique properties. To date, no report is available on the synthesis of aGQDs using KOH chemical activation; hence, their distinctive properties are yet to be revealed. In line with the intensive research on GQDs and activated carbon nanomaterial, we report here for the □rst time an ultrasonic and chemical

[a]*Integrated Polymer and Systems Engineering Group, School of Chemical and Biomolecular Engineering, The University of Sydney, NSW 2006, Australia. E-mail: v.gomes@usyd.edu.au; Fax: +61 293512854; Tel: +61 293514868*

[b]*Laboratory for Sustainable Technology, School of Chemical and Biomolecular Engineering, The University of Sydney, NSW 2006, Australia*

[c]*Intelligent Polymer Research Institute, ARC Centre of Excellence for Electromaterials Science, AIIM Facility, Innovation Campus, University of Wollongong, N. Wollongong, NSW 2522, Australia*

treatment approach for the preparation of aGQDs. Unlike their weakly luminescent non-activated counterparts of similar surface states (O/C ratio), edge-enriched aGQDs are expected to emit stronger luminescence and enhanced electrochemical double layer capacitance. Our focus here is the possible facile synthesis of aGQDs, investigation of their potentially useful attributes and comparison with non-activated GQDs, graphene and activated graphene.

Experimental

Materials

Expanded graphite was procured from Asbury Graphite (USA) and most chemicals from Sigma Aldrich (Australia). Dialysis membranes were purchased from Spectra/Pro Biotech.

Synthesis of FLGs and aFLGs

Few layer graphene sheets (FLGs) were synthesized as per our previously reported work.[16] Brie□y, a dispersion was prepared in 20 mL distilled water by mixing 0.1 wt% expanded graphite (EG) with variable amounts of sodium dodecyl sulfate (SDS) surfactant. The resulting mixture was sonicated for 60–80 min at room temperature. Sonication processes were carried out with a tip horn sonicator (Branson 450D) with a cylindrical tip (10 mm end cap diameter). The output power was 30 W of delivered power at 1650–1800 J min^{-1} level. The vial with the sample was placed in an ice bath during sonication to counter any temperature rise. About 90 wt% graphene was separated by centrifugation and sedimentation to obtain 1–10 layer graphene (FLG).

Weighed 100 mg equivalent FLGs with 100 mL aqueous dispersion was placed in a sonication bath while 30 mL of 7 M aqueous KOH solution was added dropwise for 30 min, followed by overnight soaking under stirring conditions. The extra KOH solution was removed by brie□y □ltering the mixture through a PTFE membrane (Whatman, 0.2 mm). The mixture was dried in the lab at 85 °C for 24 hours. The dry FLG/KOH mixture was heated at 800 °C for 2 hours in a horizontal tube furnace with an argon □ow of 150 sccm (STP) and working pressure of ~400 Torr. The temperature was ramped up from room temperature to 800 °C at 5 °C min^{-1}. A□er cooling in a vacuum, the sample was transferred to a 1 : 10 HCl–water solution (500 mL) and washed with DI water under centrifugation at 6000 rpm until the pH of the suspension was about 7. Then the sample was dried at 65 °C in air for 2 hours, followed by thermal annealing at 800 °C in a vacuum (0.1 Torr) for 2 hours, to generate activated FLG powders (aFLGs).

Synthesis of aGQDs and GQDs

The pristine solution with aGQDs was prepared by adding 10 mg aFLGs to a 20 mL ethanol–H_2O (1 : 1 v/v ratio) solution followed by 2 hours of tip horn ultrasonication under conditions similar to those described for aFLGs. The suspension was □ltered through a 0.22 mm microporous membrane to remove tracts of aFLGs. The mixture was further dialyzed in a dialysis bag (retained molecular weight: 3500 Da) and aGQDs having bluish □uorescence were obtained (yield *ca.* 16.3 wt%). Similarly GQDs were collected (yield *ca.* 3.4 wt%) by using FLGs as input instead of aFLGs.

Characterisation

The FLGs, aFLGs and aGQDs were examined by SEM (FESEM, Zeiss ultra Plus, 5 kV) and TEM (JEM 1400, JEOL, Japan) at accelerating voltage up to 120 kV. Raman spectra were recorded using an Invia Raman spectrometer (Renishaw plc, UK) with a laser excitation wavelength of 514 nm. X-ray photoelectron spectroscopy (XPS) measurement was conducted with ESCA LAB250Xi (ThermoScienti□c, UK) with X-ray source of monochromated Al Ka and power of 164 W (10.8 mA and 15.2 kV). The UV-vis absorption and photoluminescence spectra of GQDs were characterized using Varian Cary 50 and FluoroLog FL3-22 spectrophotometers (JY Horiba Inc.), respectively. Nitrogen sorption measurements were performed with ASAP2020 (Micromeritics, USA) to obtain the BET-speci□c surface area, pore size distribution, and total pore volume.

For electrical characterization, the working electrodes were fabricated by mixing samples of aGQDs, GQDs, aFLGs, and FLGs (separately) with poly(tetra□uoroethylene) or PTFE in a mass ratio of 90 : 10 and dispersed in ethanol. The resulting mixture was coated onto a glassy carbon electrode (GCE) by a drop-casting method and dried at 60 °C for 2 h in a vacuum oven. The mass of each electrode was 0.1 mg for thin □lms and 5 mg for thick □lms, excluding the conducting binder. The samples coated on the GCE were directly used as working electrodes in a three-electrode test cell with Pt wire as the counter electrode and Ag/AgCl as the reference electrode. Cyclic voltammetetry (CV) and galvanostatic charge–discharge were measured using a Biologic SP300 digital electrochemical workstation with potential window from −0.2 to 0.7 V in 1 M H_2SO_4 electrolyte.

Results and discussion

To produce homogeneous aGQDs, micrometer-sized few layer graphene sheets (FLGs) were used as starting materials. These were treated with KOH for activation a□er direct ultrasonication as shown schematically in Fig. 1. Samples of FLGs (<10 layers)

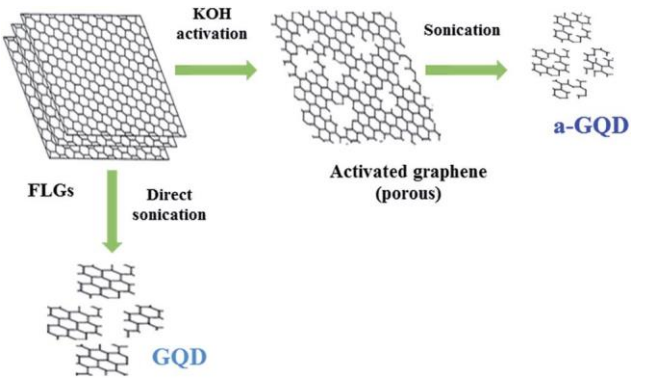

Fig. 1 Steps for preparing GQDs and aGQDs from FLGs.

were synthesized by the method we developed earlier.[16] Fig. 2 shows the TEM images of our synthesized FLGs with a red arrow indicating that few layers have formed (Fig. 2a). Fig. 2b shows that the actual size of FLGs is in the range of 6–8 mm. Their (002) estimated interlayer spacing of 3.42 Å (Fig. 1c) is slightly larger than that of bulk graphite (3.35 Å).[16] Since few layers of graphene are stacked together through weak van der Waals forces and p–p interactions, further exfoliation can simultaneously exfoliate as well as slice FLGs into large scale single-layered graphene with reduced size (<100 nm) for producing quantum dots.[17] The FLGs were activated by sodium dodecyl sulfate (SDS) assisted by KOH soaking followed by argon and vacuum annealing. After chemical activation, the FLGs became smaller, about 200 nm^{-3} mm, with pronounced, protruded edges (Fig. 2c).

The activation with KOH generated nanoscale pores in the form of bound edges on the basal plane of graphene sheets which preferentially anchor ionic charges to improve electrochemical performance compared to chemically reduced graphene.[11] Fig. 3 shows annular bright field scanning transmission electron microscopy (ABF-STEM) (Fig. 3a) images of a micron-size activated graphene sheet, and a corresponding high-resolution ABF-STEM image (Fig. 3b) of the area (red circle) marked in Fig. 3a. These images clearly indicate that the activation process etches the FLGs and generates a network of ultra-fine pores, in the size range of less than 1–7 nm throughout the sheet.

The presence of nano-pores results in somewhat fragile graphene sheets that are vulnerable to chemical attack. Ultrasonic waves with alternating low and high pressures are able to propagate fractures into the porous zones of FLGs and rip the bridged porous structures into reduced sizes to produce GQDs (Fig. 1, right). Zhou *et al.*[18] recently exfoliated inorganic graphene analogues of 2D materials (MoS_2, WS_2 and BN) in a low boiling point ethanol–H_2O mixture (1 : 1 v/v ratio) using an ultrasonic process and produced a highly stable suspension. We adapted this mixed-solvent strategy to obtain a homogeneous dispersion of GQDs. The higher yield of aGQDs (16.3 wt%) compared to GQDs (3.4 wt%) from direct sonication of FLGs clearly shows the ease of disintegration due to chemical etching of graphene sheets. The yield is found to be superior compared to methods for synthesizing GQDs directly from unoxidized graphitic precursors.[19] Fig. 4a shows a TEM image of aGQD obtained after isolation *via* dialysis, showing a relatively narrow size distribution between 1 to 8 nm (Fig. 4b).

The high resolution TEM (HRTEM) image (Fig. 4c) of an aGQD contains pores on its basal plane. These pores are marked by red arrows along with an edge pore denoted by a blue arrow; however, such nanopores have not been observed for typical GQDs.[19] Despite the presence of pores in aGQDs, the Fast Fourier transform (FFT) (Fig. 4d) of the corresponding HRTEM (Fig. 4c) shows the diffraction pattern of electrons. This implies that there is preservation of the p–p conjugated and sp^2 bonded interconnected networks of a carbon skeleton. Characterization of the edge structure (*e.g.*, zigzag and armchair) in graphene is important for understanding GQD properties. Reports show that graphene with zigzag edges offers unique optoelectronic and magnetic properties.[20]

Fig. 4e shows an HRTEM image of the edge side (green arrow point) for aGQD depicted in Fig. 4c. The GQD edges are predominantly parallel to the zigzag orientation as shown by the adjacent schematic presentation (indicated by blue arrow),

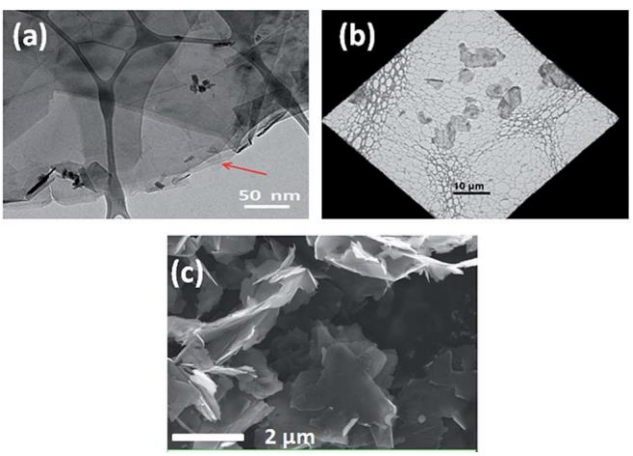

Fig. 2 (a) Magnified TEM image of few layer graphene sheets (50 nm scale); (b) TEM image of FLGs of 6–8 mm size; (c) SEM image of aFLGs with protruding edges.

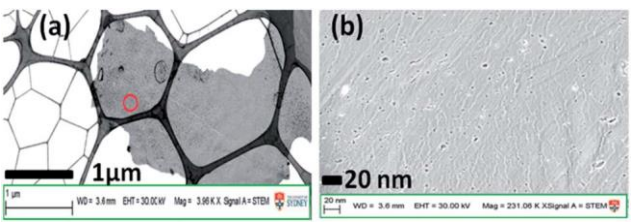

Fig. 3 (a) Low magnification ABF-STEM image of an activated gra- phene sheet; (b) high resolution ABF-STEM image of area (red circle) marked in (a). (For a clearer view of the nanopores, readers are referred to the magnified image, Fig. 1S in the ESI.†)

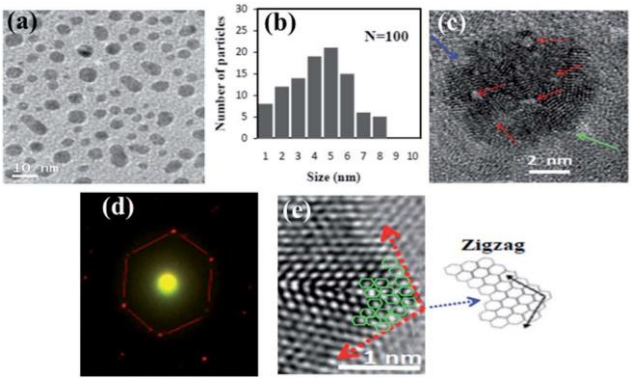

Fig. 4 (a) TEM image of aGQDs; (b) size distribution of synthesized aGQDs; (c) high resolution TEM image of a typical aGQD; (d) 2D FFT of aGQD; (e) HRTEM image of the edge of aGQD (highlighted by a green arrow in (c)) with a schematic representation of the zigzag edge termination of HRTEM image.

although other orientations are also possible. A schematic suggesting the structure of this GQD is shown in the inset of Fig. 4e. Based on the GQDs we analyzed using the HRTEM, we found that our as-prepared GQDs preferentially orient themselves in zigzag edge patterns rather than the armchair one. In accord with the unzipping mechanism of graphitic frames into tiny entities,[21] we conclude that the breakup of porous planar graphitic domains is likely initiated along the zigzag direction due to the propagation of alternating ultrasonic shock waves.

The chemical composition and structural conversion of each sample were characterized by Raman and X-ray photoemission (XPS) spectroscopy. To determine any difference in the chemical composition of GQDs and aGQDs, we measured the XPS C1s spectra (Fig. 5a). The deconvolution of peaks at 284.3 eV originates from the sp^2 hybridized graphitic carbon,[22] while the peak at 285.1 eV can be associated with sp^2 hybridized carbon bonded to carbon with defects.[23] We note that the "defect peak" with an energy shift of 0.2–1.5 eV relative to the sp^2 hybridized graphitic carbon bond is sometimes mistakenly considered as the C–C (sp^3) bond. This peak is usually located at 285.1 eV and is often found in nanodiamond films and amorphous carbon.[24] Further, the similar intensification of the 285.1 eV peak and D/G in Raman spectra (Fig. 5b), observed for both aGQDs and GQDs relative to their graphene precursors, likely indicate the presence of enhanced graphene domain edges and defects that originate from the severance of carbon bonds in graphene due to sonication.[25] On the other hand, no noticeable differences are observed with respect to the other peaks for all samples at 286.4, 287.8, and 288.9 eV, which correspond to the C–O (epoxy and alkoxy), C=O (carbonyl), and –COOH (carboxylic) groups, respectively.

The intensity of exposed edges is characterized by the D/G ratio of Raman spectra where the effect of functional groups on the surface is suppressed.[11] No noticeable differences in C–O (epoxy and alkoxy), C=O (carbonyl), and –COOH (carboxylic) groups on the surface states of our samples were observed (Fig. 5a). Thus, the change in D/G ratio (Fig. 5b) can be ascribed mainly to the physical and structural changes in the graphene skeleton. On direct sonication of FLGs, there was a slight increase in the value of *R* (the intensity of the D band divided by the intensity of the G band) of GQDs as well as similarities in the half width at half-maximum (HWHM) values for both bands. These are due to the significant edge structural evolution from FLGs to crystalline GQDs. However, the higher *R* value and larger HWHM of the D band of aFLGs and aGQDs compared to FLGs and GQDs indicate the formation of greater exposed edge-sites which directly contribute to the intensification of the D band. In addition, the peak at 1620 cm^{-1} has evolved to a greater extent for both aFLGs and aGQDs. This can be associated with edge-enriched planes due to the formation of pores along with edges at the free end.[26]

The optical properties of aGQDs and GQDs (Fig. 6) were determined using the UV-vis PL and PL excitation (PLE) measurements. Fig. 6a shows the PL spectra of the GQD (0.01 mg mL^{-1}) and aGQD (0.01 mg mL^{-1}) in aqueous suspensions. Compared to GQDs, aGQDs show stronger PL emission. The PL peak intensity of aGQDs was about 4.6 times higher than that of GQDs. Moreover under irradiation by a 365 nm Xenon lamp (16 W), both GQDs and aGQDs emitted blue luminescence (photographic images, Fig. 6a, inset) which suggest that they share the same source for their luminescence.[2] This phenomenon can be attributed to their exposed edge states[5] as their oxygen-containing functional groups are significantly suppressed during the activation process as observed *via* XPS measurements (Fig. 5a).

Nanoscale pores on graphene are able to open band gaps due to the localization of electron–hole pairs at the pore edges.[27] This implies that in addition to free edges, the sub-nanometer pores in aGQDs (Fig. 4b) contribute significantly towards the observed intense blue PL emission of aGQDs compared to its non-activated counterpart. Thus, the relatively smaller isolated sp^2-hybridized islands formed by the pores in aGQD basal

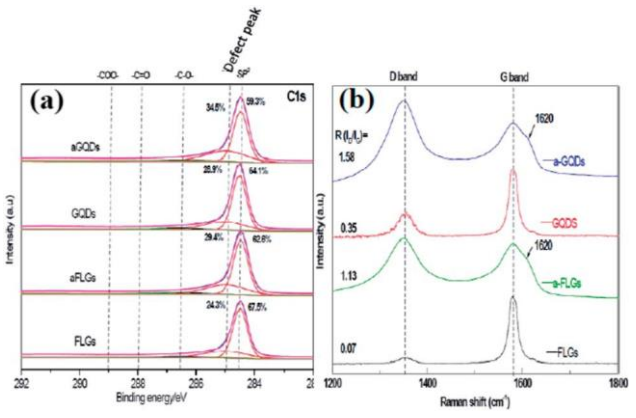

Fig. 5 (a) XPS C1s spectra; (b) Raman spectra for FLGs, aFLGs, GQDs and aGQDs.

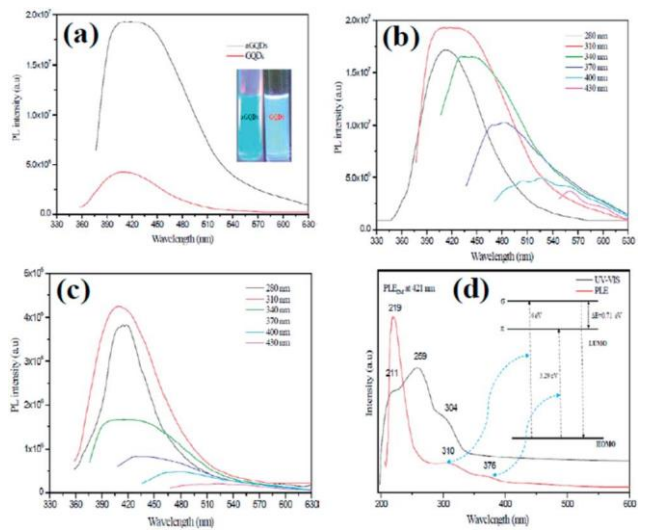

Fig. 6 (a) PL spectra of GQDs and aGQDs (0.01 mg ml^{-1} in an ethanol–H_2O mixture of 1 : 1 v/v ratio). Inset: digital images of blue PL emissions of GQDs and aGQDs under 365 nm UV light (right). Emission spectra with excitations at different wavelengths for: (b) aGQDs and (c) GQDs. (d) UV and PLE spectra of aGQDs with emission mechanism.

planes possibly contribute towards the high PL intensity which is consistent with the trends observed with other quantum dots having properties attributable to the quantum confinement effect at small particle size (1–10 nm).[28] Both the synthesized aGQDs (Fig. 6b) and GQDs (Fig. 6c) exhibit excitation-dependent PL behavior. With an excitation wavelength variation from 280 to 430 nm, the PL peak shifts to longer wavelengths and the strongest peaks for both materials are observed with excitation at 310 nm. The strongest peak of aGQDs is blue-shifted to 421 from 409 nm (for GQD), which indicates that different types of electronically excited states exist for these two materials.

For the measured UV-vis spectra (Fig. 6d), bands 259 and 360 cm^{-1} indicate newly opened band gaps arising from triple carbenes at the zigzag edges, corresponding to transitions from the highest occupied molecular orbits (HOMOs) to the s and p orbitals of the lowest unoccupied molecular orbits (LUMOs) of triple carbenes, respectively.[4a] The PL excitation spectra recorded at the highest emission wavelength (l_{em} ¼ 421 nm) are shown in Fig. 6d. These spectra comprise one peak at (a) 219 nm (5.66 eV), and two shoulders at (b) 310 nm (4.0 eV) and (c) 376 nm (3.71 eV). The highest energy peak is assigned to an absorption band corresponding to p–p* transition. The carbene ground-state multiplicity is related to energy differences (D*E*) between the s and p orbital. D*E* is typically below 1.5 eV for a triplet ground state.[29] Since the estimated D*E* (0.71 eV) is less than 1.5 eV, the two transitions in bands 310 nm and 376 nm in the PLE spectra (Fig. 6d) can be assigned to triplet carbene at the zigzag edges of graphene. Thus, the prepared aGQDs are expected to exhibit unique optoelectronic properties arising from the nanoscale pores and zigzag edge emissive sites in their quantum structure.

To determine the surface area and pore-size distribution of GQDs, nitrogen adsorption measurements were carried out using the ASAP2020 (Micromeritics, USA) instrument. Fig. 7 presents the nitrogen adsorption isotherms of treated and untreated graphene nanosheets together with the corresponding pore-size distributions. Increase in surface area and pore size of graphitic carbon materials have been reported following chemical activation by KOH.[9] Here, a significant change in surface areas of aFLGs (1289 $m^2\ g^{-1}$) and aGQDs (1502 $m^2\ g^{-1}$) were observed compared to their non-activated counterparts of FLGs (69 $m^2\ g^{-1}$) and GQDs (268 $m^2\ g^{-1}$). The larger surface areas of GQDs and aGQDs compared to the precursor materials (FLGs & aFLGs) are due to the disintegration of the precursors into smaller fractions with greater exposed edges resulting from extended exfoliation *via* ultrasonication in the ethanol–water mixture.

The pore-size distribution of aGQDs shows a sharp peak of 0.5 nm for nanopores, a relatively narrow peak of 2 nm, as well as mesopores around 3 and 4 nm (Fig. 7b). But such nanopores (<1 nm, inset, Fig. 7b) are not observed in GQDs. The mesopores for both samples originate from loose stackings, entanglements and overlaps of the GQD/aGQD sheets, while pores having diameters less than 1 nm stem from pores present in the sheets (Fig. 4b). Well-defined ultra-fine pores (<1 nm) of aGQDs are highly beneficial[30] for the transport and diffusion of ions during the fast charge–discharge process, and facilitate enhanced electrochemical performance.

Activation of carbon nanomaterials with KOH to produce a-CNTs[10] and a-graphene[11] have been reported to show promise as supercapacitor electrodes. For aGQDs, apart from their unique luminescent properties, the edge-enriched states are also expected to contribute towards their electrochemical energy storage capacity in applications of supercapacitor electrodes. Combining the structure (sp^2) of graphene with the quantum confinement and edge effects of carbon-dots, GQDs could enhance the energy storage by the effective scavenging of ions and transport of electrons through their tiny sp^2 scaffold.

The supercapacitive performances of the prepared samples were evaluated with a three-electrode cell configuration where a glass carbon electrode (GCE) was used as the current collector. Cyclic voltammograms (CVs) of all four samples were measured with a potential window of 0.9 V at a scan rate of 20 mV s^{-1} in 1 M H_2SO_4 aqueous electrolyte (Fig. 8a). The CV profile of FLGs and GQDs exhibited smooth profiles with no apparent peaks, whereas the appearance of weak redox peaks for aFLGs and

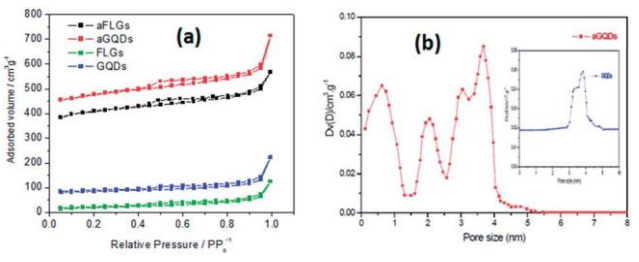

Fig. 7 (a) Nitrogen adsorption/desorption isotherms recorded at −196 °C; (b) BJH pore size distribution of aGQDs (inset shows data for GQDs).

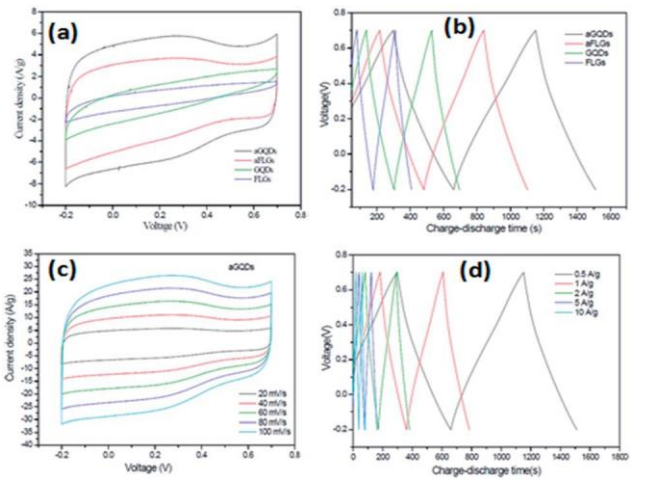

Fig. 8 (a) Current density *versus* voltage profiles at 20 mV; (b) comparison of CV based on charge–discharge curves at 0.5 A g^{-1}; (c) cyclic voltammetry of aGQDs at 20–100 mV s^{-1} scan rates; and (d) charge–discharge curves of aGQDs at 0.5–10 A g^{-1}.

aGQDs can be ascribed to protonation *via* their enriched free zigzag sites by the acidic medium and due to the formation of complexes between H^+ and zigzag sites.[31]

Fig. 8c reveals the CV profiles of aGQDs at scan rates ranging from 20 to 100 mV s^{-1}. With increasing scan rates, we observed that similar CV profiles were maintained, indicating good wetting and ease of access by ions.[32] To determine the specific capacitance of three electrode materials, galvanostatic charge–discharge (C–D) measurements were carried out and are shown in Fig. 8b for the four samples at a current density of 0.5 A g^{-1}. The charge curves were nearly symmetric with respect to their corresponding discharge curves for the potential range tested. This indicates a high degree of reversibility between the charge and discharge processes.

The charge–discharge curves of aGQD and aFLG films on the GCE electrode showed small deviations from linearity, due to the protonation phenomena compared to less edge-enriched FLGs and GQDs. The specific capacitance calculated from the discharge curves of the aGQD film on the GCE was 236 F g^{-1}, which is greater than that of aFLGs (172 F g^{-1}), GQDs (108 F g^{-1}) and FLGs (63 F g^{-1}). The galvanostatic C–D curves of aGQDs at current densities of 1–10 A g^{-1} (Fig. 8d) present consistent profile shapes, indicating that the aGQD film is stable over a wide range of current flows, and only 1.17% of the specific capacitance is degraded even at a high current density of 10 A g^{-1}.

Our findings indicate that the edge enriched aFLGs and aGQDs generate enhanced electrode capacitance due to the improved accessibility of electrolyte ions through both the bound and free end edges, since the edge sites have the ability to accumulate more charges than the basal plane.[33] Further, thicker films having greater mass (5 mg) for all four samples (aGQDs, aFLGs, GQDs, and FLGs) were also tested under similar electrochemical conditions and their corresponding capacitances are presented in the ESI (Fig. 2S†). Though deviations in capacitance are observed due to the increase of charge transfer resistance and the slower ion diffusion in the thicker electrode, the capacitance values are of similar magnitude, and the hierarchy in capacitance values for all samples (aGQDs > aFLGs > GQDs > FLGs), both thin and thick films, are maintained. These results indicate that chemically activated graphene quantum dots with lower mass loading could be beneficial for applications for the next generation of miniaturized energy storage devices such as electrochemical micro-supercapacitors. Additional data on cyclo-voltammetry and charge–discharge responses for thick films are presented in the ESI (Fig. 3S and 4S†).

Conclusions

We developed a simple yet effective strategy using ultra-sonication and chemical activation to generate activated GQDs having enriched edges, which show photo-luminescence similar in origin to their non-activated counterparts but distinctive in their higher intensity. Activating GQDs with KOH provides an effective method to enhance and tune their intrinsic photoluminescence and electrochemical properties for use in advanced applications. Compared to GQDs, the synthesized aGQDs had BET surface area enhanced by a factor of six, the photoluminescence intensity by about four times and electro-capacitance by a factor of about two. Thus, the synthesized aGQDs possess superior electro-chemical energy storage capacity for application as electrodes for supercapacitors, while the enhanced edge effects of aGQDs giving rise to intense photo-luminescence are useful for applications such as bio-imaging, light-emitting diodes and optoelectronics.

Acknowledgements

The authors acknowledge partial support from an ARC Linkage grant, a scholarship (MH) and a University of Sydney Post-doctoral Fellowship (KRR).

Notes and references

1 (*a*) L. L. Li, G. H. Wu, G. H. Yang, J. Peng, J. W. Zhao and J. J. Zhu, *Nanoscale*, 2013, 5, 4015; (*b*) J. H. Shen, Y. H. Zhu, X. L. Yang and C. Z. Li, *Chem. Commun.*, 2012, 48, 3686.
2 F. Liu, M.-H. Jang, H. D. Ha, J.-H. Kim, Y.-H. Cho and T. S. Seo, *Adv. Mater.*, 2013, 25, 3657.
3 S. Zhu, J. Zhang, X. Liu, B. Li, X. Wang, S. Tang, Q. Meng, Y. Li, C. Shi, R. Hu and B. Yang, *RSC Adv.*, 2012, 2, 2717.
4 (*a*) D. Pan, J. Zhang, Z. Li and M. Wu, *Adv. Mater.*, 2010, 22, 734; (*b*) J. Peng, W. Gao, B. K. Gupta, Z. Liu, R. Romero-Aburto, L. Ge, L. Song, L. B. Alemany, X. Zhan, G. Gao, S. A. Vithayathil, B. A. Kaipparettu, A. A. Marti, T. Hayashi, J.-J. Zhu and P. M. Ajayan, *Nano Lett.*, 2012, 12, 844.
5 K. Lingam, R. Podila, H. Qian, S. Serkiz and A. M. Rao, *Adv. Funct. Mater.*, 2013, 23, 5062.
6 H. Sun, L. Wu, W. Wei and X. Qu, *Mater. Today*, 2013, 16, 434.
7 H. Kalita, V. Harikrishnan, D. B. Shinde, K. V. Pillai and M. Aslam, *Appl. Phys. Lett.*, 2013, 102, 143104.
8 H. Marsh and F. Rodriguez-Reinoso, *Activated Carbon*, Elsevier, London, 2006.
9 J. Wang and S. Kaskel, *J. Mater. Chem.*, 2012, 22, 23710.
10 E. Raymundo-Pinero, P. Azais, T. Cacciaguerra, D. Cazorla-Amoros, A. Linares-Solano and F. Beguin, *Carbon*, 2005, 43, 786.
11 Y. Zhu, S. Murali, M. D. Stoller, K. J. Ganesh, W. Cai, P. J. Ferreira, A. Pirkle, R. M. Wallace, K. A. Cychosz, M. Thommes, D. Su, E. A. Stach and R. S. Ruoff, *Science*, 2011, 332, 153.
12 (*a*) X. Zhang, J. Xin and F. Ding, *Nanoscale*, 2013, 5, 2556; (*b*) Y. H. Kim, T. Hayashi, J. H. Kim and M. Endo, *J. Energy Chem.*, 2013, 22, 183.
13 (*a*) A. Ambrosi, A. Bonanni and M. Pumera, *Nanoscale*, 2011, 3, 2256; (*b*) T. J. Davies, M. E. Hyde and R. G. Compton, *Angew. Chem., Int. Ed.*, 2005, 44, 5121.
14 (*a*) S. Banerjee, J. Shim, J. Rivera, X. Jin, D. Estrada, V. Solovyeva, X. You, J. Pak, E. Pop, N. Aluru and R. Bashir, *ACS Nano*, 2013, 7, 834; (*b*) W. Yuan, Y. Zhou, Y. Li, C. Li, H. Peng and J. Zhang, *Nat. Sci. Rep.*, 2013, 3, 2248.
15 K. A. Ritter and J. W. Lyding, *Nat. Mater.*, 2009, 8, 235.

16 M. Hassan, K. R. Reddy, E. Haque, A. I. Minett and V. G. Gomes, *J. Colloid Interface Sci.*, 2013, 410, 43.
17 S. Zhuo, M. Shao and S. T. Lee, *ACS Nano*, 2012, 6, 1059.
18 K. Zhou, N. Mao, H. Wang, Y. Peng and H. Zhang, *Angew. Chem., Int. Ed.*, 2011, 50, 10839.
19 L. Lin and S. Zhang, *Chem. Commun.*, 2012, 48, 10177.
20 (*a*) L. R. Radovic and B. Bockrath, *J. Am. Chem. Soc.*, 2005, 127, 5917; (*b*) V. P. Gusynin, V. A. Miransky, S. G. Sharapov, I. A. Shovkovy and C. M. Wynberg, *Phys. Rev. B: Condens. Matter Mater. Phys.*, 2009, 79, 115431; (*c*) K. Nakada, M. Fujita, G. Dresselhaus and M. S. Dresselhaus, *Phys. Rev. B: Condens. Matter Mater. Phys.*, 1996, 54, 17954.
21 D. V. Kosynkin, A. L. Higginbotham, A. Sinitskii, J. R. Lomeda, A. Dimiev, B. K.Price and J. M. Tour, *Nature*, 2009, 458, 872.
22 H. Yu, Y. Jin, F. Peng, H. Wang and J. Yang, *J. Phys. Chem. C*, 2008, 112, 6758.
23 (*a*) H. Estrade-Szwarckopf, *Carbon*, 2004, 42, 1713; (*b*) G. Bepete, D. Voiry, M. Chhowalla, Z. Chiguvare and N. J. Coville, *Nanoscale*, 2013, 5, 6552–6557.
24 K. L. Ma, J. X. Tang, Y. S. Zou, Q. Ye, W. J. Zhang and S. T. Lee, *Appl. Phys. Lett.*, 2007, 90, 92105.
25 D. Yang, A. Velamakanni, G. Bozoklu, S. Park, M. Stoller, R. D. Piner, S. Stankovich, I. Jung, D. A. Field, C. A. Ventrice Jr and R. S. Ruoff, *Carbon*, 2009, 47, 145.
26 (*a*) T. C. Chieu, M. S. Dresselhaus and M. Endo, *Phys. Rev. B: Condens. Matter Mater. Phys.*, 1982, 26, 5867; (*b*) G. Katagiri, H. Ishida and A. Ishitani, *Carbon*, 1988, 26, 565.
27 J. Bai, X. Zhong, S. Jiang, Y. Huang and X. Duan, *Nat. Nanotechnol.*, 2010, 5, 190.
28 D. V. Melnikov and J. R. Chelikowsky, *Phys. Rev. Lett.*, 2004, 92, 46802.
29 R. Hoffmann, *J. Am. Chem. Soc.*, 1968, 90, 1475.
30 J. Chmiola, G. Yushin, Y. Gogotsi, C. Portet, P. Simon and P. L. Taberna, *Scienc*, 2006, 313, 1760.
31 D. Bourissou, O. Guerret, F. P. Gabbai and G. Bertrand, *Chem. Rev.*, 2000, 100, 39.
32 Z. Lin, Y. Liu, Y. Yao, O. J. Hildreth, Z. Li, K. Moon and C. P. Won, *J. Phys. Chem. C*, 2011, 115, 7120.
33 C. Portet, G. Yushin and Y. Gogotsi, *Carbon*, 2007, 45, 2511.